https://doi.org/10.5194/acp-2020-225
Preprint. Discussion started: 17 March 2020

Atmospheric Chemistry and Physics Discussions

Drivers of cloud droplet number variability in the summertime Southeast United States

Aikaterini Bougiatioti[1,2], Athanasios Nenes[2,3,4], Jack J. Lin[2,a], Charles A. Brock[5], Joost A. de Gouw[5,6,b], Jin Liao[5,6,c,d], Ann M. Middlebrook[5], André Welti[5,6,e]

[1]Institute for Environmental Research & Sustainable Development, National Observatory of Athens, P. Penteli, GR-15236, Greece
[2]School of Earth & Atmospheric Sciences, Georgia Institute of Technology, Atlanta, GA 30332, USA
[3]Laboratory of Atmospheric Processes and their Impacts, School of Architecture, Civil & Environmental Engineering, École Polytechnique Fédérale de Lausanne, CH-1015, Lausanne, Switzerland
[4]Institute for Chemical Engineering Sciences, Foundation for Research and Technology Hellas, Patras, GR-26504, Greece
[5]Chemical Sciences Division, NOAA Earth System Research Laboratory, Boulder, CO, 80305, USA
[6]Cooperative Institute for Research in Environmental Sciences, Univ. of Colorado, Boulder, CO, 80309, USA
[a] now at: Nano and Molecular Systems Research Unit, Box 3000, FI-90014 University of Oulu, Oulu, Finland
[b] now at: Department of Chemistry and Biochemistry, University of Colorado Boulder, Boulder, CO, USA
[c] now at: Atmospheric Chemistry and Dynamic Laboratory, NASA Goddard Space Flight Center, Greenbelt, MD, USA
[d] now at: Universities Space Research Association, GESTAR, Columbia, MD, USA
[e] now at: Atmospheric Composition Research Unit, Finnish Meteorological Institute, Helsinki, Finland

Correspondence to: Aikaterini Bougiatioti (abougiat@noa.gr), Athanasios Nenes (athanasios.nenes@epfl.ch).

Abstract

The Southeast United States has experienced a different climate warming trend compared to other places worldwide. Several hypotheses have been proposed to explain this trend, one being the interaction of anthropogenic and biogenic aerosol precursors that synergistically promote aerosol formation, elevate cloud droplet concentration and induce regional cooling. We examine these aerosol-cloud droplet links by analyzing regional scale data collected onboard the NOAA WP-3D aircraft during the 2013 Southeast Nexus (SENEX) campaign to quantify the sensitivity of droplet number to aerosol number, chemical composition and vertical velocity on a regional scale. The observed aerosol size distributions, chemical composition and vertical velocity distribution (Gaussian with standard deviation σ_w) are introduced into a state-of-the-art cloud droplet parameterization to show that cloud maximum supersaturations in the region are low, ranging from 0.02 to 0.52% with an average of 0.14±0.05%. Based on these low values of supersaturation, the majority of activated droplets correspond to particles of diameter 90 nm and above. Droplet number shows little sensitivity to total aerosol owing to their strong competition for water vapor. Given, however, that σ_w exhibits considerable diurnal variability (ranging from 0.16 m s^{-1} during nighttime to over 1.2 m s^{-1} during day), its covariance with total aerosol number (N_a) during the same period amplifies

https://doi.org/10.5194/acp-2020-225
Preprint. Discussion started: 17 March 2020

Atmospheric Chemistry and Physics Discussions

predicted response in cloud droplet number (N_d) by 3 to 5 times. Therefore, correct consideration of vertical velocity and its covariance with time and aerosol amount is important for fully understanding aerosol-cloud interactions and the magnitude of the aerosol indirect effect. Datasets and analysis such as the one presented here can provide the required constraints for addressing this important problem.

1. Introduction

Atmospheric particles (aerosols) interact with the incoming solar radiation through scattering and absorption processes which tend to cool the Earth, especially over dark surfaces such as oceans and forests (Brock et al., 2016a). Aerosols also act as cloud condensation nuclei (CCN) and subsequently form cloud droplets and indirectly affect climate through modification of cloud radiative properties - an effect which constitutes one of the most uncertain aspects of anthropogenic climate change (Seinfeld et al., 2016). Studies often highlight the importance of constraining the aerosol size distribution, particle composition and mixing state for predicting CCN concentrations (Cubison et al., 2008; Quinn et al., 2008). Model assumptions often cannot consider the full complexity required to comprehensively compute CCN – which together with other emissions and process uncertainties lead to CCN prediction errors that can be significant (e.g., Fanourgakis et al., 2019). Owing to the sublinear response of cloud droplet number concentration (N_d) to aerosol perturbations, prediction errors in CCN generally result in errors in N_d which are less than those for CCN (Fanourgakis et al., 2019). The sublinear response arises because elevated CCN concentration generally increases the competition of the potential droplets for water vapor; this in turn depletes supersaturation and the N_d that can eventually form (Reutter et al., 2009; Bougiatioti et al., 2016; Fanourgakis et al., 2019; Kalkavouras et al., 2019). A critically important parameter is the vertical velocity; so important in fact that droplet number variability may be driven primarily by vertical velocity variations (Kacarab et al., 2020; Sullivan et al., 2019). Compared to aerosols, vertical velocity is much less observed, constrained and evaluated in aerosol-cloud interaction studies, hence may be a source of persistent biases in models (Sullivan et al., 2019).

The Southeast United States (SEUS) presents a particularly interesting location for studying regional climate change, as it has not considerably warmed over the past 100 years – except for the last decade (Carlton et al., 2018; Yu et al., 2014; Leibensperger et al., 2012b). These trends are in contrast with the trends observed in most locations globally (IPCC 2013), and several hypotheses have been proposed to explain this regional phenomenon, including the effect of involving short-lived climate forcers such as secondary aerosols combined with the enhanced humidity in the region and their impact on clouds (Carlton et al., 2018; Yu et al., 2014). Here, we analyze data collected during the Southeast Nexus of Air Quality

https://doi.org/10.5194/acp-2020-225
Preprint. Discussion started: 17 March 2020


Atmospheric Chemistry and Physics Discussions

and Climate (SENEX) campaign in June-July 2013, which was the airborne component led by the National Oceanic and Atmospheric Administration (NOAA), of a greater measurement campaign throughout the SEUS, the Southeast Atmosphere Study (SAS; Carlton et al., 2018). Here we analyze data collected onboard the NOAA WP-3D and apply a state-of-the-art droplet parameterization to determine the maximum supersaturation and N_d achieved in cloudy updrafts, for all science flights with available number size distribution and chemical composition data. We also determine the sensitivity of droplet formation to vertical velocity and aerosol, with the purpose of understanding the drivers of droplet variability in the boundary layer of the SEUS by obtaining regional-scale, representative values of the relationship between the driving parameters and cloud droplet number.

2. Methods

2.1 Aircraft instrumentation

The analysis utilizes airborne, in situ data collected during the June-July 2013 SENEX mission, aboard the National Oceanic and Atmospheric Administration (NOAA) WP-3D aircraft (typical airspeed ~100 m s^{-1}) based in Smyrna, Tennessee (36º00'32''N, 86º31'12''W). In total, twenty research flights were conducted. Based on the availability of the relevant data described below, thirteen flights are analyzed in this work. Description of the analyzed research flights are provided in Table 1. Detailed information on the instrumentation and measurement strategy during the SENEX campaign can be found in Warneke et al. (2016).

Dry particle number distributions from 4 - 7000 nm were measured using multiple condensation and optical particle counters. 4-700 nm particles were measured by a nucleation mode aerosol size spectrometer (NMASS; Warneke et al., 2016) and an ultra-high sensitivity aerosol spectrometer (UHSA; Brock et al., 2011), while for larger particles with dry diameters between 0.7 and 7.0 μm, a custom-built white-light optical particle counter (WLOPC) was used.

Measurements of the composition of submicron vacuum aerodynamic diameter non-refractory aerosol (less than 0.7 μm diameter) were made with a Compact Time-of-Flight Aerosol Mass Spectrometer (C-ToF-AMS; Aerodyne, Billerica, Massachesetts, US) (Canagaratna et al., 2007; Kupc et al., 2018) customized for aircraft use, with a 10 s time resolution (Warneke et al., 2016). Particles entering the instrument are focused and impacted on a 600 ºC inverted-cone vaporizer. The volatilized vapors are analyzed by electron ionization mass spectrometry, providing mass loadings of sulfate, nitrate, organics, ammonium and chloride. For the C-ToF-AMS, the transmission efficiency of particles between 100 and 700 nm is assumed to be 100% through the specific aerodynamic focusing lens used while mass concentrations are calculated

https://doi.org/10.5194/acp-2020-225
Preprint. Discussion started: 17 March 2020


Atmospheric Chemistry and Physics Discussions

using a chemical composition-dependent collection efficiency (Middlebrook et al., 2012; Wagner et al., 2015). The C-ToF-AMS only measures non-refractory aerosol chemical composition, therefore this analysis provides mass loadings of sulfate, nitrate, ammonium and organic constituents with a 10 s time resolution and neglects the contribution of black carbon (BC). The calculation of the average volume fractions from the mass loading follows that of Moore et al. (2012). An average organic density of 1.4 g cm^{-3} is used, characteristic of aged aerosol (Moore et al., 2011; Lathem et al., 2013) while for the inorganic species the respective densities are used, assuming the aerosol to be internally mixed.

The aircraft was equipped by the NOAA Aircraft Operations Center (AOC) flight facility, incorporating a suite of instruments to provide information on exact aircraft position as well as numerous meteorological parameters (Warneke et al., 2016). The analysis in this work makes use of vertical wind velocity, aircraft radar altitude, and ambient temperature, pressure and relative humidity (RH) provided by NOAA AOC. Location of the instrumentation on the aircraft can be found elsewhere (Warneke et al., 2016). For measurements inside the fuselage a low turbulence inlet (Wilson et al., 2004) and sampling system (Brock et al., 2011; 2016a) was used to decelerate the sample flow to the instruments. The C-ToF-AMS was connected downstream of an impactor with 50% efficiency at a 1.0 μm aerodynamic diameter (PM1) cut-point (Warneke et al., 2016).

2.2 Aerosol hygroscopicity parameter

The aerosol hygroscopicity parameter (Petters and Kreidenweis, 2007), κ, is calculated assuming a mixture of an organic and inorganic component with volume fraction ε_{org}, ε_{inorg} and characteristic hygroscopicity κ_{org}, $\kappa_{inorg,}$ respectively ($\kappa=\varepsilon_{inorg}\kappa_{inorg}+\varepsilon_{org}\kappa_{org}$). The organic and inorganic volume fraction are derived from the C-ToF-AMS data. Since throughout the summertime SEUS, aerosol inorganic nitrate mass and volume fraction are very low (Weber et al., 2016; Fry et al., 2018), κ_{inorg} =0.6, representative for ammonium sulfate, is used. For the organic fraction, a hygroscopicity value of κ_{org}=0.14 is used, based on concurrent measurements conducted at the ground site of the SAS at the rural site of Centreville, Alabama (Cerully et al., 2015). This value is also in accordance with the cumulative result of studies conducted in the Southeast US using measurements of droplet activation diameters in subsaturated regimes, providing κ_{org} of > 0.1 (Brock et al., 2016a).

2.3 Cloud droplet number and maximum supersaturation

Using the observed aerosol number size distribution (1 s time resolution) and the hygroscopicity derived from the chemical composition measurements (10 s time resolution), we calculate the droplet number (N_d) and maximum supersaturation (S_{max}) that would form in clouds in the airmasses sampled. Droplet number

https://doi.org/10.5194/acp-2020-225
Preprint. Discussion started: 17 March 2020


Atmospheric Chemistry and Physics Discussions

and maximum supersaturation calculations are carried out at a regional scale using an approach similar to that of Bougiatioti et al. (2016) and Kalkavouras et al. (2019) with the sectional parameterization of Nenes and Seinfeld (2003), later improved by Barahona et al. (2010) and Morales Betancourt and Nenes (2014a). A sectional representation of the size distribution is used and provided for each data point of each flight (per second, e.g. for Flight 5, n=23213 data points). Given that chemical composition is provided with a 10 s time resolution, the same hygroscopicity values are used for 10 size distributions during each flight. Temperature and pressure required for droplet number calculations are obtained from the NOAA AOC flight facility dataset.

Droplets form from activation of aerosol in cloudy updrafts, so here we use the available measurements of vertical velocity together with the aerosol measurements to derive a potential cloud droplet concentration. Given that vertical velocity varies considerably inside the boundary layer we represent droplet number with the average concentration that results from integrating over the distribution (probability density function, PDF) of observed updraft velocities. To accomplish this, each flight is divided in segments where the aircraft flew at a constant height. For each segment, the positive vertical velocities are fit to a Gaussian distribution with mean of zero and width of spectral dispersion σ_w. Positive vertical velocities ("updrafts") were used, as they are the part of the vertical velocity spectrum that is responsible for cloud droplet formation. The σ_w values derived from the level leg segments are then averaged into one single σ_w value (and standard deviation) to represent the flight. Application of the "characteristic velocity" approach (Morales and Nenes, 2010) then gives the PDF-averaged droplet number concentration by calling the droplet parameterization at a single "characteristic" velocity, $w^*=0.79\sigma_w$ (Morales and Nenes, 2010). This calculation approach is applied to each size distribution measured. Apart from its theoretical basis, this methodology has shown to provide closure with observed droplet numbers in ambient clouds (e.g. Kacarab et al., 2020).

In determining σ_w, we consider segments that are expected to be in the boundary layer: 91 % of the segments are below 1000 m (mean altitude ~700 m; Table 2) typically corresponding to the height of the boundary layer in the summertime US (Seidel et al., 2013). The vertical velocity distributions observed gave σ_w =0.97±0.21 m s^{-1} for daytime flights, and σ_w =0.23±0.04 m s^{-1} for nighttime flights (Table 2). Because of this strong diurnal variation in σ_w, potential droplet formation is evaluated at four vertical velocities that cover the observed ranged, namely 0.1, 0.3, 0.6 and 1 m s^{-1}.

We also compute the sensitivity of the derived N_d, to changes in aerosol number concentration (N_a), κ and σ_w, expressed by the partial derivatives $\partial N_d/\partial N_a$, $\partial N_d/\partial \kappa$ and $\partial N_d/\partial \sigma_w$ computed from the parameterization using a finite difference approximation (Bougiatioti et al., 2016; Kalkavouras et al., 2019). These sensitivities, together with the observed variance in N_a, κ, and σ_w are also used to attribute droplet number

https://doi.org/10.5194/acp-2020-225
Preprint. Discussion started: 17 March 2020


Atmospheric Chemistry and Physics Discussions

variability to variations in the respective aerosol and vertical velocity parameters following the approach of Bougiatioti et al. (2016) and Kalkavouras et al. (2019).

3. Results and Discussion

3.1. Particle composition and size distribution

For the determination of the different aerosol species present, neutral and acidic sulfate species are distinguished by the molar ratio of ammonium to sulfate ions. A molar ratio higher than 2 indicates the presence of only ammonium sulfate, while values between 1 and 2 indicate the presence of both ammonium sulfate and bisulfate (Seinfeld and Pandis, 1998). For most of the flights, the molar ratio of ammonium versus sulfate was well above 2, having a mean value of 2.41±0.72 (median 2.06). For the nighttime flights the values were somewhat lower (1.91±0.42 and median of 1.85, respectively). Nevertheless, ammonium sulfate is always the predominant sulfate salt. Organic mass fractions for the SENEX research flights are provided in Table 1. Overall, organic aerosol was found to dominate during all flights, contributing 66%-75% of the total aerosol volume. Most of the remaining aerosol volume consists of ammonium sulfate, ranging from 12%-39% (with a mean of 23%±6%). The organic mass fraction during the flights was found to decrease with height (see Fig. 1). This vertical variability of the chemical composition can have a strong impact on droplet number within the boundary layer, as air masses from aloft may descend and interact with that underneath. Figure 1 represents the organic mass fractions during Flights 5 and 12. The lowest organic mass fractions overall were observed during Flight 12 (35%±18% with values < 5% for altitudes >3000 m, Fig.1b) while the highest ones were observed at flights over predominantly rural areas (Flights 5 (Fig. 1c) , 10 and 16). During Flight 5 the organic mass fraction was high (68%±5%), with the highest values found in the free troposphere at altitudes > 3000 m. High organic mass fractions were also found during a nighttime flight that included portions of the Atlanta metropolitan area, with values up to 78%. The impact of the chemical variability on droplet number is discussed in section 3.2.

The predominance of the organic fraction is also reflected in the hygroscopicity parameter values, with an overall κ = 0.25±0.05, which is close to the proposed global average of 0.3 (Seinfeld and Pandis, 1998). The highest values are, as expected, for flights exhibiting the lowest organic mass fraction, namely Flight 12 with a κ = 0.39 (Table 2). The rest of the κ-values are close to the overall values, as the organic mass fractions are around 0.65.

Median aerosol size distributions are obtained from the median and interquartile range in each size bin from the aerosol size distribution measurements during segments where the aircraft flew at a constant height. The impact of the variability of the total aerosol number on droplet number is discussed in detail further in

https://doi.org/10.5194/acp-2020-225
Preprint. Discussion started: 17 March 2020


Atmospheric Chemistry and Physics Discussions

section 3.2. Overall, number concentrations ranged from around 500 to over 100000 cm^{-3} with number size distributions varying markedly over the course of a flight. In general, free tropospheric distributions exhibited characteristics of a bimodal distribution with a prominent broad accumulation mode peak (80-200 nm) and an Aitken mode peak (30-60 nm) (Fig. 2a) while boundary layer size distributions exhibited a more prominent accumulation mode (Fig. 2b). There was considerable variability in the contributions of the nucleation, Aitken, and accumulation modes to the total aerosol number, depending on altitude and proximity to aerosol sources (Fig. 2c). Nevertheless, the modal diameters did not vary much. Distributions during nighttime flights exhibited similar total aerosol number and variability; nevertheless, size distributions were more complex exhibiting even three different modes (20-40, 70-100 and 130-200 nm; Fig. 2d). Considering that mostly particles in the accumulation mode activate into cloud droplets (particles with diameters >90 nm), contrasts between day and nighttime aerosol characteristics/variability may not be as large, and driven primarily by the total aerosol number in the accumulation mode.

3.2 Potential cloud droplet number

The calculation of N_d and S_{max}, was carried out for all thirteen research flights. Results are given in Tab. 3 for the four different values (0.1, 0.3, 0.6 and 1 m s^{-1}) of σ_w. Overall it can be seen that for all flight conditions and for low σ_w, N_d shows a low variance (mean of 132±20 for 0.1 m s^{-1} and 350±100 for 0.3 m s^{-1}). For a given σ_w, the variance of N_d is predominantly attributed to relative changes in N_a rather than changes in the chemical composition (expressed by changes in the hygroscopicity parameter, κ). The highest relative contribution of the chemical composition (12% and 35% for 0.1 and 0.3 m s^{-1}, respectively) to the variation of N_d is found for Flight 18, during which the total aerosol number was the lowest. Indicative of a "cleaner" environment; the organic mass fraction was relatively lower and the hygroscopicity parameter was higher. Even though the lowest organics mass fraction and highest κ were observed during Flight 12, droplet formation is much more sensitive to changes in aerosol concentration than to variations in composition.

As the vertical velocity increases, so does supersaturation and consequently the droplet number (by 62% from 0.1 to 0.3 m s^{-1}, 70% from 0.3 to 0.6 m s^{-1} and another 39% from 0.6 to 1 m s^{-1}). The relative contribution of the chemical composition to the variation of cloud droplet number increases from 5±3% for 0.1 m s^{-1}, to 12.3±8% for 0.3 m s^{-1}, to 14.5±10% for 0.3 m s^{-1} and 16.5±9% for 1 m s^{-1}. The highest droplet numbers are estimated for Flights 6 and 10, which included urban environments during daytime (Atlanta). Overall during daytime, when σ_w varies little and is large, and N_a is high, the relative contribution of N_a to the variation of N_d is the highest (more than 90%) while the relative contribution of κ is limited (less than 10%) (see Table 3, Flights 10, 11, 12, 17 and 19). Turbulence is limited during nighttime when σ_w is the

https://doi.org/10.5194/acp-2020-225
Preprint. Discussion started: 17 March 2020


Atmospheric Chemistry and Physics Discussions

231 lowest (0.23±0.04); therefore, the σ_w = 0.3 m s^{-1} case is most representative of nighttime conditions. During
232 daytime, when σ_w is high (0.97±0.21), σ_w = 1 m s^{-1} should be considered as most representative.

233 As σ_w varies considerably throughout the day, we estimate its contribution together with variations in N_a
234 and κ, to the total variability in N_d based on $\partial N_d/\partial\kappa$, $\partial N_d/\partial N_a$ and $\partial N_d/\partial\sigma_w$ and the variances of κ, N_a and σ_w
235 (Table 4). The σ_w variation during nighttime, although small (always less than 10%), consistently remains
236 an important contributor to N_d variability, because droplet formation tends to be in the updraft velocity-
237 limited regime. At higher values of σ_w (Table 4), the contribution of σ_w variability to N_d variability is reduced
238 and dominated by N_a variability.

239 To explore the importance of aerosol compared to updraft velocity, we focus on two pairs of flights
240 conducted in two sectors, from each sector one during day- and one during night-time (see Fig.3). In both
241 pairs of flights (Flight 5 and 15, and Flight 6 and 9), σ_w varies about the same between night and day (Table
242 4). For the first pair of flights, the daytime variability in N_d (which is 69%) is to within 75% driven by
243 aerosol (69% by N_a and 7% from κ) and 24% by σ_w. For nighttime, 58% by aerosol (51% by N_a and 7%
244 from κ) and 42% of the variability is driven by σ_w. For the second pair of night/day flights, N_a is on average
245 similar, σ_w varies by a factor of 4.0 and κ varies by 13%. Attribution calculations suggest that the diurnal
246 variability in N_d (where daytime values are 72.1% higher than nighttime) is 3, 54 and 43% for κ, N_a and σ_w,
247 respectively during day and 7, 76, and 17% driven by κ, N_a and σ_w, respectively during night (Table 4). In
248 the second sector, 57% of the variability in N_d is driven by aerosol during the day and 83% during the night.

249 As expected, droplet number (N_d) and maximum supersaturation (S_{max}) increases as σ_w becomes larger. The
250 highest S_{max} are around 0.2-0.3% and found for flights which exhibited large and highly variable σ_w (Flights
251 4, 5, 12 and 19) while the lowest S_{max} are around 0.10% and found for the nighttime flights (Flights 9, 15
252 and 16). All other flights yield similar S_{max}, which are around 0.13%. Based on the calculated S_{max} for every
253 flight, the majority of the activated droplets correspond to particles of 90 nm diameter and above. Figure 3
254 presents the calculated N_d for the four aforementioned flights, namely Fights 5 (Fig. 3a), 15 (Fig. 3b), 6
255 (Fig. 3c) and 9 (Fig. 3d) using the observed σ_w. The size of the markers represents the number of droplets,
256 while the color scale the respective total aerosol number.

257 Figure 4 shows N_d relative to N_a for flights conducted in two sectors, during day and night (Flights 5 & 15,
258 and Flights 6 & 9, respectively). It can be seen that throughout these flights, N_d reaches a plateau, where
259 any additional aerosol does not translate to any significant increase in N_d. This plateau is caused by strong
260 water vapor limitations and is different for day and night. S_{max} is lower during night because vertical wind
261 velocity, ambient T and RH are lower. The same factors cause that for Flight 6 & 9 (Fig. 4c & d) where N_a
262 was almost the same, N_d is almost 3.5 times lower during night (Flight 9). For the whole dataset (13 flights),

https://doi.org/10.5194/acp-2020-225
Preprint. Discussion started: 17 March 2020


Atmospheric Chemistry and Physics Discussions

results are summarized in Figure 5, where droplet numbers are calculated based on the observed σ_w and the respective "characteristic", mean velocities, w^*. Under low w^* conditions, N_a variability does not result in an important change in N_d. On the contrary, when w^* tends to increase and N_a increases, as is characteristic of polluted regions, during daytime, then the impact on droplet number is more notable. This point is evident in Figure 6, comprising the different segments of the flights when the aircraft sampled at practically the same altitude within the boundary layer. It can be seen that N_a is enhanced as w^* increases. The lowest w^* values (shaded area) correspond to the segments of the flights during nighttime.

Overall, S_{max} of clouds from all the evaluated SENEX data, is 0.14±0.05%. Tripling σ_w from 0.1 to 0.3 m s^{-1} results in 31% increase in S_{max}, while doubling from 0.3 to 0.6 m s^{-1} results in 26.2% increase in S_{max} and a further σ_w increase to 1 m s^{-1} leads to an additional 20.7% increase in S_{max}. Overall effect of updraft velocity on calculated N_d: tripling σ_w from 0.1 to 0.3 m s^{-1} results in a 61.9% increase in N_d, doubling from 0.3 to 0.6 m s^{-1} results in a 40.5% N_d increase; increasing σ_w to 1 m s^{-1} leads to an additional 26.9% increase in N_d. Furthermore, for a given σ_w, despite of the presence or not of a large number of aerosol (e.g. Flight 10 where N_a is 2.7 times higher than N_a in Flight 15) the difference in calculated N_d for 0.6 m s^{-1} is only 1.3 times higher for Flight 10 than Flight 15. This highlights the relative insensitivity of N_d to variations in N_a for constant σ_w.

4. Summary and Conclusions

Measurements of wind velocity, ambient conditions (*T, RH*), aerosol number size distribution and composition in the SEUS obtained during the SENEX 2013 project are used to analyze the drivers of droplet formation. Overall 13 research flights are studied, covering environments over sectors with different aerosol sources, impacting total aerosol number, size distribution and chemical composition. Aerosol volume is largely dominated by an organic fraction resulting in a calculated hygroscopicity of 0.25±0.05.

Based on the calculation of cloud droplet number concentration (N_d) and maximum supersaturation (S_{max}), we find that on a regional scale, most of the variability of N_d is due to the fluctuations in N_a (Table 4), in accordance with other recent studies (Fanourgakis et al., 2019). Nonetheless, N_d levels are also sensitive to fluctuations in σ_w, as a variation by a factor of 4.0 in σ_w may lead to an N_d variation of almost a factor of 3.6 and at the same time the N_d response to different N_a levels may be enhanced by a factor of 5 (Figure 4). S_{max} changes in response to aerosol concentration, in a way that tends to partially mitigate N_d responses to aerosol. Overall, maximum supersaturation levels remain quite low (0.14±0.05%) with predicted levels being much lower in lower altitudes (0.05±0.1%). Because of the strong competition for water vapor (expressed by the low S_{max}), cloud droplet number exhibits enhanced sensitivity to aerosol number

https://doi.org/10.5194/acp-2020-225
Preprint. Discussion started: 17 March 2020


Atmospheric Chemistry and Physics Discussions

295 variations throughout the flights, regardless of aerosol composition. On the other hand, droplet
296 concentration especially within the boundary layer approaches a "plateau" that is strongly driven by vertical
297 velocity (turbulence) and the resulting supersaturation, but also aerosol concentration. In "cleaner"
298 environments where total aerosol number is lower, the relative contribution of vertical velocity to cloud
299 droplet number is almost half during nighttime (24% vs. 42% during daytime) while the relative
300 contribution of N_a to the variance in N_d is somewhat higher (69% vs. 51% during daytime) even though N_a
301 is 2-fold lower during night. On the contrary, in environments with elevated concentrations of
302 accumulation-mode particles, the majority of cloud droplet number variations (54% during nighttime vs.
303 76% during daytime) can be attributed to changes in total aerosol number and to a lesser extent to vertical
304 velocity (43% during nighttime vs. 17% during daytime). The relative contribution of the total aerosol
305 number to the cloud droplet number dominates over variations in chemical composition (expressed by κ).
306 There are cases however where chemical composition variability contributes a non-negligible (~9%)
307 contribution to droplet number variability.

308 Overall, our results show that atmospheric dynamics is a key driver of cloud droplet formation and its
309 variability in the region. Especially in cases when the boundary layer turbulence is low (e.g. during
310 nighttime), low vertical velocity, generating only small supersaturation, can be as important a contributor
311 to droplet number variability as aerosol number. For cases with high vertical velocities and high aerosol
312 number concentration, it is the aerosol concentration that dominates the variability in cloud droplet number.
313 On average, the two variables (N_a and σ_w) contribute almost equally to the variability in cloud droplet
314 number concentration (N_d) and together account for more than 90% of variability. This finding is consistent
315 with recent modeling studies noting the importance of vertical velocity variability as a driver of the temporal
316 variability of global hydrometeor concentration (Morales Betancourt and Nenes, 2014b; Sullivan et al.,
317 2016). Furthermore, the N_d enhancement from changes in N_a is magnified up to 5 times from concurrent
318 changes in σ_w. A similar situation has also been observed in smoke-influenced marine boundary layers in
319 the S.Atlantic (Kacarab et al., 2020). Altogether, these findings carry important implications for model
320 assessments of aerosol indirect climate forcing (e.g., Leibensperger et al., 2012a) and aerosol-cloud
321 interaction studies using remote sensing, as patterns of cooling (although consistent with aerosol and cloud
322 fields) may omit the covariance of vertical velocity with aerosol number, therefore neglecting this important
323 driver of hydrometeor variability.

324 **Data Availability:** The data used in this study can be downloaded from the NOAA public data repository
325 at https://www.esrl.noaa.gov/csd/projects/senex/. The Gaussian fits used for determining σ_w and the droplet
326 parameterization used for the calculations in the study are available from athanasios.nenes@epfl.ch upon
327 request.

https://doi.org/10.5194/acp-2020-225
Preprint. Discussion started: 17 March 2020

Atmospheric Chemistry and Physics Discussions

Author Contributions: conceptualization, A.B. and A.N.; methodology, A.B. and A.N.; software, A.N.; formal analysis, A.B. and A.N.; investigation, A.B., A.N. and J.J.L.; data curation, A.B., J.J.L., C.B., J.A.G., J.L., A.M.M., A.W.; writing—original draft preparation, A.B. and A.N.; writing—review and editing, A.B., A.N., J.J.L., C.B., A.W., additional comments by A.M.M.; visualization, A.B. A.N. and J.J.L.; supervision, A.N.; project administration, A.N.; funding acquisition, A.N.

Funding: This study was supported by the Environmental Protection Agency STAR Grant R835410, the Action "Supporting of Postdoctoral Researchers" of the Operational Program "Education and Lifelong Learning" (action's beneficiary: General Secretariat for Research and Technology) and is co-financed by the European Social Fund (ESF) and the Greek State. We also acknowledge funding from the European Research Council, CoG-2016 project PyroTRACH (726165) funded by H2020-EU.1.1. – Excellent Science.

Conflicts of Interest: The authors declare no conflict of interest.

References

Barahona, D., West, R.E.L., Stier, P., Romakkaniemi, S., Kokkola, H., and Nenes, A.: Comprehensively accounting for the effect of giant CCN in cloud activation parameterizations, Atmos. Chem. Phys., 10, 2467–2473, doi:10.5194/acp-10-2467-2010, 2010.

Bougiatioti, A., Bezantakos, S., Stavroulas, I., Kalivitis, N., Kokkalis, P., Biskos, G., Mihalopoulos, N., Papayannis, A., and Nenes, A.: Biomass-burning impact on CCN number, hygroscopicity and cloud formation during summertime in the eastern Mediterranean, Atmos. Chem. Phys., 16, 7389–7409, https://doi.org/10.5194/acp-16-7389-2016, 2016.

Bougiatioti, A., Argyrouli, A., Solomos, S., Vratolis, S., Eleftheriadis, K., Papayannis, A., and Nenes, A.: CCN activity, variability and influence on droplet formation during the HygrA-Cd campaign in Athens, Atmosphere, 8, 108, https://doi.org/10.3390/atmos8060108, 2017.

Brock, C. A., Cozic, J., Bahreini, R., Froyd, K. D., Middlebrook, A. M., McComiskey, A., Brioude, J., Cooper, O. R., Stohl, A., Aikin, K. C., de Gouw, J. A., Fahey, D. W., Ferrare, R. A., Gao, R. S., Gore, W., Holloway, J. S., Hübler, G., Jefferson, A., Lack, D. A., Lance, S., Moore, R. H., Murphy, D. M., Nenes, A., Novelli, P. C., Nowak, J. B., Ogren, J. A., Peischl, J., Pierce, R. B., Pilewskie, P., Quinn, P. K., Ryerson, T. B., Schmidt, K. S., Schwarz, J. P., Sodemann, H., Spackman, J. R., Stark, H., Thomson, D. S., Thornberry, T., Veres, P., Watts, L. A., Warneke, C., and Wollny, A. G.: Characteristics, sources, and transport of aerosols measured in spring 2008 during the aerosol,

https://doi.org/10.5194/acp-2020-225
Preprint. Discussion started: 17 March 2020

radiation, and cloud processes affecting Arctic Climate (ARCPAC) Project, Atmos. Chem. Phys., 11, 2423–2453, 2011.

Brock, C. A., Wagner, N. L., Anderson, B. E., Attwood, A. R., Beyersdorf, A., Campuzano-Jost, P., Carlton, A. G., Day, D. A., Diskin, G. S., Gordon, T. D., Jimenez, J. L., Lack, D. A., Liao, J., Markovic, M. Z., Middlebrook, A. M., Ng, N. L., Perring, A. E., Richardson, M. S., Schwarz, J. P., Washenfelder, R. A., Welti, A., Xu, L., Ziemba, L. D., and Murphy, D. M.: Aerosol optical properties in the southeastern United States in summer – Part 1: Hygroscopic growth, Atmos. Chem. Phys., 16, 4987-5007, https://doi.org/10.5194/acp-16-4987-2016, 2016a.

Canagaratna, M. R., Jayne, J. T., Jimenez, J. L., Allan, J. D., Alfarra,M. R., Zhang, Q., Onasch, T. B., Drewnick, F., Coe, H., Middlebrook, A., Delia, A., Williams, L. R., Trimborn, A. M., Northway, M. J., DeCarlo, P. F., Kolb, C. E., Davidovits, P., and Worsnop, D. R.: Chemical and microphysical characterization of ambient aerosols with the aerodyne aerosol mass spectrometer, Mass Spectrometry Reviews, 26, 185–222, 2007.

Carlton, A.G., J.A. de Gouw, J.L. Jimenez, J.L. Ambrose, A.R. Attwood, S. Brown, K.R. Baker, C. Brock, R.C. Cohen, S. Edgerton, C. Farkas, D. Farmer, A.H. Goldstein, L. Gratz, A. Guenther, S. Hunt, L. Jaeglé, D.A. Jaffe, J. Mak, C. McClure, A. Nenes, T.K.V. Nguyen, J.R. Pierce, S. de Sa, N.E. Selin, V. Shah, S. Shaw, P.B. Shepson, S. Song, J. Stutz, J. Surratt, B.J. Turpin, C. Warneke, R.A. Washenfelder, P.O. Wennberg, and Xianling Zhou: A synthesis of the southeast atmosphere studies: coordinated investigation of fundamental atmospheric chemistry questions, Bulletin of the American Meteorological Society, doi: 10.1175-BAMS-D-16-0048.1, 2018.

Cubison, M. J., Ervens, B., Feingold, G., Docherty, K. S., Ulbrich, I. M., Shields, L., Prather, K., Hering, S., and Jimenez, J. L.: The influence of chemical composition and mixing state of Los Angeles urban aerosol on CCN number and cloud properties, Atmos. Chem. Phys., 8, 5649-5667, https://doi.org/10.5194/acp-8-5649-2008, 2008.

DeCarlo, P. F., Kimmel, J. R., Trimborn, A., Northway, M. J., Jayne, J. T., Aiken, A. C., Gonin, M., Fuhrer, K., Horvath, T., Docherty, K. S., Bates, D. R., and Jimenez, J. L.: Field-Deployable, High-Resolution, Time-of-Flight Aerosol Mass Spectrometer, Anal. Chem., 78, 8281–8289, doi:8210.1021/ac061249n, 2006.

Fanourgakis, G. S., Kanakidou, M., Nenes, A., Bauer, S. E., Bergman, T., Carslaw, K. S., Grini, A., Hamilton, D. S., Johnson, J. S., Karydis, V. A., Kirkevåg, A., Kodros, J. K., Lohmann, U., Luo, G., Makkonen, R., Matsui, H., Neubauer, D., Pierce, J. R., Schmale, J., Stier, P., Tsigaridis, K., van Noije, T., Wang, H., Watson-Parris, D., Westervelt, D. M., Yang, Y., Yoshioka, M., Daskalakis, N., Decesari, S., Gysel-Beer, M., Kalivitis, N., Liu, X., Mahowald, N. M., Myriokefalitakis, S., Schrödner, R., Sfakianaki, M., Tsimpidi, A. P., Wu, M., and Yu, F.: Evaluation of global simulations of aerosol

https://doi.org/10.5194/acp-2020-225
Preprint. Discussion started: 17 March 2020

particle and cloud condensation nuclei number, with implications for cloud droplet formation, Atmos. Chem. Phys., 19, 8591–8617, https://doi.org/10.5194/acp-19-8591-2019, 2019.

Fry, J. L., Brown, S. S., Middlebrook, A. M., Edwards, P. M., Campuzano-Jost, P., Day, D. A., Jimenez, J. L., Allen, H. M., Ryerson, T. B., Pollack, I., Graus, M., Warneke, C., de Gouw, J. A., Brock, C. A., Gilman, J., Lerner, B. M., Dubé, W. P., Liao, J., and Welti, A.: Secondary organic aerosol (SOA) yields from NO3 radical + isoprene based on nighttime aircraft power plant plume transects, Atmos. Chem. Phys., 18, 11663-11682, https://doi.org/10.5194/acp-18-11663-2018, 2018.

Cerully, K. M., Bougiatioti, A., Hite, Jr., J. R., Guo, H., Xu, L., Ng, N. L., Weber, R., and Nenes, A.: On the link between hygroscopicity, volatility, and oxidation state of ambient and water-soluble aerosols in the southeastern United States, Atmospheric Chemistry and Physics, 15, 8679–8694, 2015.

IPCC (Intergovernmental Panel on Climate Change): Climate Change 2013: The Physical Science Basis, Summary for Policymakers, Cambridge University Press, Cambridge, UK and New York, 2013.

Kacarab, M., Thornhill, K. L., Dobracki, A., Howell, S. G., O'Brien, J. R., Freitag, S., Poellot, M. R., Wood, R., Zuidema, P., Redemann, J., and Nenes, A.: Biomass burning aerosol as a modulator of the droplet number in the southeast Atlantic region, Atmos. Chem. Phys., 20, 3029–3040, https://doi.org/10.5194/acp-20-3029-2020, 2020.

Kalkavouras, P., Bossioli, E., Bezantakos, S., Bougiatioti, A., Kalivitis, N., Stavroulas, I., Kouvarakis, G., Protonotariou, A. P., Dandou, A., Biskos, G., Mihalopoulos, N., Nenes, A., and Tombrou, M.: New particle formation in the southern Aegean Sea during the Etesians: importance for CCN production and cloud droplet number, Atmos. Chem. Phys., 17, 175-192, https://doi.org/10.5194/acp-17-175-2017, 2017.

Kalkavouras, P., Bougiatioti, A., Kalivitis, N., Stavroulas, I., Tombrou, M., Nenes, A., and Mihalopoulos, N.: Regional new particle formation as modulators of cloud condensation nuclei and cloud droplet number in the eastern Mediterranean, Atmos. Chem. Phys., 19, 6185–6203, https://doi.org/10.5194/acp-19-6185-2019, 2019.

Kupc, A., Williamson, C., Wagner, N. L., Richardson, M., and Brock, C. A.: Modification, calibration, and performance of the Ultra-High Sensitivity Aerosol Spectrometer for particle size distribution and volatility measurements during the Atmospheric Tomography Mission (ATom) airborne campaign, Atmos. Meas. Tech., 11, 369–383, https://doi.org/10.5194/amt-11-369-2018, 2018.

Lathem, T. L., Beyersdorf, A. J., Thornhill, K. L., Winstead, E. L., Cubison, M. J., Hecobian, A., Jimenez, J. L., Weber, R. J., Anderson, B. E., and Nenes, A.: Analysis of CCN activity of Arctic aerosol and Canadian biomass burning during summer 2008, Atmos. Chem. Phys., 13, 2735-2756, https://doi.org/10.5194/acp-13-2735-2013, 2013.

https://doi.org/10.5194/acp-2020-225
Preprint. Discussion started: 17 March 2020

426 Leibensperger, E. M., Mickley, L. J., Jacob, D. J., Chen, W.-T., Seinfeld, J. H., Nenes, A., Adams, P. J.,
427 Streets, D. G., Kumar, N., and Rind, D.: Climatic effects of 1950–2050 changes in US anthropogenic
428 aerosols – Part 1: Aerosol trends and radiative forcing, Atmos. Chem. Phys., 12, 3333-3348,
429 https://doi.org/10.5194/acp-12-3333-2012, 2012a.
430 Leibensperger, E. M., Mickley, L. J., Jacob, D. J., Chen, W.-T., Seinfeld, J. H., Nenes, A., Adams, P. J.,
431 Streets, D. G., Kumar, N., and Rind, D.: Climatic effects of 1950–2050 changes in US anthropogenic
432 aerosols – Part 2: Climate response, Atmos. Chem. Phys., 12, 3349-3362, https://doi.org/10.5194/acp-
433 12-3349-2012, 2012b.
434 Middlebrook, A. M., Bahreini, R., Jimenez, J. L., and Canagaratna, M. R.: Evaluation of Composition-
435 Dependent Collection Efficiencies for the Aerodyne Aerosol Mass Spectrometer using Field Data,
436 Aerosol Sci. Tech., 46, 258–271, doi.org/10.1080/02786826.2011.620041, 2012.
437 Moore, R. H., Bahreini, R., Brock, C. A., Froyd, K. D., Cozic, J., Holloway, J. S., Middlebrook, A. M.,
438 Murphy, D. M., and Nenes, A.: Hygroscopicity and composition of Alaskan Arctic CCN during April
439 2008, Atmos. Chem. Phys., 11, 11 807–11 825, 2011.
440 Moore, R. H., Cerully, K., Bahreini, R., Brock, C. A., Middlebrook, A. M., and Nenes, A.: Hygroscopicity
441 and composition of California CCN during summer 2010, J. Geophys. Res., 117, 2012.
442 Morales, R. and Nenes, A.: Characteristic updrafts for computing distribution-averaged cloud droplet
443 number, autoconversion rate effective radius, J. Geophys. Res., 115, D18220,
444 doi:10.1029/2009JD013233, 2010.
445 Morales Betancourt, R. and Nenes, A.: Droplet activation parameterization: the population-splitting
446 concept revisited, Geosci. Model Dev., 7, 2345–2357, https://doi.org/10.5194/gmd-7-2345-2014,
447 2014a.
448 Morales Betancourt, R. and Nenes, A.: Understanding the contributions of aerosol properties and
449 parameterization discrepancies to droplet number variability in a global climate model, Atmos. Chem.
450 Phys., 14, 4809-4826, https://doi.org/10.5194/acp-14-4809-2014, 2014b.
451 Nenes, A. and Seinfeld, J.H.: Parameterization of cloud droplet formation in global climate models, J.
452 Geophys. Res, 108, 4415, doi:10.1029/2002JD002911, 2003.
453 Petters, M. D. and Kreidenweis, S. M.: A single parameter representation of hygroscopic growth and cloud
454 condensation nucleus activity, Atmos. Chem. Phys., 7, 1961–1971, doi:10.5194/acp-7-1961-2007,
455 2007.
456 Quinn, P. K., Bates, T. S., Coffman, D. J., and Covert, D. S.: Influence of particle size and chemistry on
457 the cloud nucleating properties of aerosols, Atmos. Chem. Phys., 8, 1029-1042,
458 https://doi.org/10.5194/acp-8-1029-2008, 2008.

https://doi.org/10.5194/acp-2020-225
Preprint. Discussion started: 17 March 2020

459 Reutter, P., Su, H., Trentmann, J., Simmel, M., Rose, D., Gunthe, S. S., Wernli, H., Andreae, M. O., and
460 Pöschl, U.: Aerosol- and updraft-limited regimes of cloud droplet formation: influence of particle
461 number, size and hygroscopicity on the activation of cloud condensation nuclei (CCN), Atmos. Chem.
462 Phys., 9, 7067-7080, https://doi.org/10.5194/acp-9-7067-2009, 2009.
463 Seidel, D. J., Zhang, Y., Beljaars, A., Golaz, J.-C., Jacobson, A. R., and Medeiros, B.: Climatology of the
464 planetary boundary layer over the continental United States and Europe, J. Geophys. Res., 117,
465 D17106, doi:10.1029/2012JD018143, 2013.
466 Seinfeld, J., and Pandis, S.: Atmospheric Chemistry and Physics: From Air Pollution to Climate Change,
467 John Wiley, Hoboken, N. J., 1998.
468 Seinfeld, J. H., Bretherton, C. S., Carslaw, K. S., Coe, H., De- Mott, P. J., Dunlea, E. J., Feingold, G., Ghan,
469 S. J., Guenther, A.B., Kahn, R. A., Kracunas, I. P., Kreidenweis, S. M., Molina, M. J., Nenes, A.,
470 Penner, J. E., Prather, K. A., Ramanathan, V., Ramaswamy, V., Rasch, P. J., Ravishankara, A. R.,
471 Rosenfeld, D., Stephens, G., and Wood R.: Improving Our Fundamental Understanding of the Role of
472 Aerosol-Cloud Interactions in the Climate System, P. Nat. Acad. Sci. USA, 113, 5781–5790,
473 https://doi.org/10.1073/pnas.1514043113, 2016.
474 Sullivan, S.C., Lee, D., Oreopoulos, L., and Nenes, A.: The role of updraft velocity in temporal variability
475 of cloud hydrometeor number, Proc.Nat.Acad.Sci, 113, 21, doi: 10.1073/pnas.1514039113, 2016.
476 Wagner, N. L., Brock, C. A., Angevine, W. M., Beyersdorf, A., Campuzano-Jost, P., Day, D., de Gouw, J.
477 A., Diskin, G. S., Gordon, T. D., Graus, M. G., Holloway, J. S., Huey, G., Jimenez, J. L., Lack, D. A.,
478 Liao, J., Liu, X., Markovic, M. Z., Middlebrook, A. M., Mikoviny, T., Peischl, J., Perring, A. E.,
479 Richardson, M. S., Ryerson, T. B., Schwarz, J. P., Warneke, C., Welti, A., Wisthaler, A., Ziemba, L.
480 D., and Murphy, D. M.: In situ vertical profiles of aerosol extinction, mass, and composition over the
481 southeast United States during SENEX and SEAC4RS: observations of a modest aerosol enhancement
482 aloft, Atmos. Chem. Phys., 15, 7085-7102, https://doi.org/10.5194/acp-15-7085-2015, 2015.
483 Warneke, C., Trainer, M., de Gouw, J. A., Parrish, D. D., Fahey, D. W., Ravishankara, A. R., Middlebrook,
484 A. M., Brock, C. A., Roberts, J. M., Brown, S. S., Neuman, J. A., Lerner, B. M., Lack, D., Law, D.,
485 Hübler, G., Pollack, I., Sjostedt, S., Ryerson, T. B., Gilman, J. B., Liao, J., Holloway, J., Peischl, J.,
486 Nowak, J. B., Aikin, K. C., Min, K.-E., Washenfelder, R. A., Graus, M. G., Richardson, M., Markovic,
487 M. Z., Wagner, N. L., Welti, A., Veres, P. R., Edwards, P., Schwarz, J. P., Gordon, T., Dube, W. P.,
488 McKeen, S. A., Brioude, J., Ahmadov, R., Bougiatioti, A., Lin, J. J., Nenes, A., Wolfe, G. M., Hanisco,
489 T. F., Lee, B. H., Lopez-Hilfiker, F. D., Thornton, J. A., Keutsch, F. N., Kaiser, J., Mao, J., and Hatch,
490 C. D.: Instrumentation and measurement strategy for the NOAA SENEX aircraft campaign as part of
491 the Southeast Atmosphere Study 2013, Atmos. Meas. Tech., 9, 3063-3093,
492 https://doi.org/10.5194/amt-9-3063-2016, 2016.

https://doi.org/10.5194/acp-2020-225
Preprint. Discussion started: 17 March 2020

Atmospheric Chemistry and Physics Discussions

493 Wilson, J. C., Lafleur, B. G., Hilbert, H., Seebaugh, W. R., Fox, J., Gesler, D. W., Brock, C. A., Huebert,
494 B. J., and Mullen, J.: Function and performance of a low turbulence inlet for sampling supermicron
495 particles from aircraft platforms, Aerosol Sci. Tech., 38, 790–802, 2004.
496 Weber RJ, Guo H, Russell AG, Nenes A.: High aerosol acidity despite declining atmospheric sulfate
497 concentrations over the past 15 years, Nat. Geosci., 9, 282-285, 2016.
498 Yu, S., Alapaty, K., Mathur, R., Pleim, J., Zhang, Y., Nolte, C., Eder, B., Foley, K., and Nagashima, T.:
499 Attribution of the United States "warming hole": Aerosol indirect effect and precipitable water vapor.
500 Sci. Rep., 4, 6929, https:// doi.org/10.1038/srep06929, 2014.

https://doi.org/10.5194/acp-2020-225
Preprint. Discussion started: 17 March 2020

Atmospheric Chemistry and Physics Discussions

Table 1: Research flights from SENEX 2013 used in this study.

Flight	Date	Local Time (CDT, UTC-5 hrs)	κ	Organic mass fraction
4	10/6	09:55-16:30	0.23±0.02	0.62±0.11
5	11/6	11:30-17:57	0.20±0.00	0.68±0.05
6	12/6	09:48-15:31	0.21±0.01	0.68±0.07
9	19/6	17:30-23:29	0.24±0.01	0.66±0.06
10	22/6	10:01-17:09	0.21±0.02	0.68±0.08
11	23/6	10:08-17:22	0.25±0.03	0.58±0.07
12	25/6	10:18-17:25	0.39±0.02	0.35±0.18
14	29/6	10:26-17:39	0.22±0.03	0.62±0.07
15	2/7	20:08-02:51	0.28±0.05	0.55±0.09
16	3/7	19:56-02:55	0.22±0.05	0.67±0.09
17	5/7	09:52-16:24	0.23±0.05	0.59±0.14
18	6/7	09:19-16:18	0.31±0.02	0.52±0.08
19	8/7	10:11-16:44	0.23±0.04	0.62±0.08

https://doi.org/10.5194/acp-2020-225
Preprint. Discussion started: 17 March 2020

Atmospheric Chemistry and Physics Discussions

505 **Table 2:** Flight number, time interval, spectral dispersion of vertical wind velocity (σ_w) and characteristic
506 vertical velocity $w^*=0.79\sigma_w$ during flight segments where the aircraft flew at a constant altitude.

Flight (pass)	Time Range	σ_w (m s^{-1})	w* (m s^{-1})	Altitude (m)	Flight (pass)	Time Range	σ_w (m s^{-1})	w* (m s^{-1})	Altitude (m)
5 (1)	12:31-12:58	1.02	0.81	549± 58	9 (1)	18:44-18:58	0.255	0.202	797±2.01
5 (2)	13:16-13:29	0.82	0.65	982±11	9 (2)	19:20-19:29	0.249	0.197	740±1.23
5 (3)	13:34-13:50	1.01	0.80	502±13	9 (3)	19:33-19:48	0.217	0.171	740±1.23
5 (4)	13:53-14:08	1.03	0.81	614±27	9 (4)	19:51-20:25	0.218	0.173	776±1.22
5 (5)	14:20-15:00	0.91	0.72	603±40	9 (5)	20:34-20:39	0.232	0.183	597±1.19
5 (6)	15:35-15:41	0.87	0.69	533±18	9 (7)	20:56-21:10	0.201	0.158	773±1.11
5 (7)	16:17-16:30	0.77	0.61	638±23	9 (8)	21:31-21:45	0.191	0.151	725±1.18
5 (8)	16:31-16:39	0.55	0.44	559±18	9 (9)	22:24-22:31	0.257	0.203	745± 1.36
5 (9)	17:10-17:22	0.53	0.42	686±40	9 (10)	22:48-22:54	0.221	0.175	804± 1.37
14 (1)	12:34-12:49	0.94	0.75	558±2	15 (1)	21:09-21:52	0.236	0.186	505±6.64
14 (2)	13:57-14:17	0.97	0.77	658±3	15 (2)	22:19-22:31	0.301	0.238	633±1.21
14 (3)	14:22-14:46	0.95	0.75	737±3	15 (3)	22:42-22:54	0.255	0.202	600±1.17
14 (4)	14:58-15:33	0.55	0.43	746±23	15 (4)	23:26-23:37	0.329	0.260	908±1.56
14 (5)	15:55-16:08	0.57	0.45	714±3	15 (5)	00:02-00:19	0.297	0.235	1208±1.23
14 (6)	16:11-16:21	0.77	0.61	801±3	15 (6)	00:43-1:08	0.253	0.199	592±1.37
14 (7)	16:33-16:41	0.45	0.35	793± 2	15 (7)	1:10-1:24	0.276	0.218	676±1.02
					15 (8)	1:37-2:02	0.207	0.164	713±19.5
12 (1)	11:50-12:34	0.96	0.75	484±3	19 (1)	11:20-11:41	0.622	0.492	1014±2.27
12 (2)	12:48-13:18	1.09	0.86	503±3	19 (2)	12:09-12:23	1.203	0.95	652±3.34
12 (3)	13:34-13:50	1.12	0.88	894±3	19 (3)	12:51-13:10	0.873	0.689	537±2.51
12 (4)	14:06-14:40	1.04	0.82	479±4	19 (4)	13:22-13:49	1.294	1.022	518±22.6
12 (5)	15:21-15:32	1.10	0.87	521±3	19 (5)	14:44-14:57	1.361	1.075	528±3.26
12 (6)	15:43-16:02	0.99	0.78	475±3	19 (6)	15:04-16:06	0.896	0.708	524±2.8

507

508

https://doi.org/10.5194/acp-2020-225
Preprint. Discussion started: 17 March 2020

Atmospheric Chemistry and Physics Discussions

509 **Table 3:** Derived cloud parameters (maximum supersaturation, droplet number) and relative contribution of chemical composition and total
510 aerosol number for different vertical velocities. Numbers in parentheses indicate standard deviation values.

511

Flight	N_a	N_a variab	σ_w=0.1 m s^{-1}				σ_w=0.3 m s^{-1}				σ_w=0.6 m s^{-1}				σ_w=1.0 m s^{-1}			
			S_{max}	N_d	Cont κ	Cont N_a	S_{max}	N_d	Cont κ	Cont N_a	S_{max}	N_d	Cont κ	Cont N_a	S_{max}	N_d	Cont κ	Cont N_a
4	6118	4520	0.11 (0.06)	122 (41)	0.08	0.92	0.16 (0.09)	315 (114)	0.20	0.80	0.21 (0.12)	520 (212)	0.23	0.77	0.26 (0.17)	737 (321)	0.2	0.8
5	4324	2598	0.08 (0.04)	139 (31)	0.09	0.91	0.1 (0.06)	388 (104)	0.15	0.85	0.14 (0.08)	712 (216)	0.17	0.83	0.17 (0.1)	1063 (360)	0.21	0.79
6	4958	3054	0.07 (0.07)	151 (24)	0.03	0.97	0.08 (0.04)	422 (70)	0.11	0.89	0.1 (0.06)	773 (171)	0.08	0.92	0.13 (0.07)	1162 (302)	0.07	0.93
9	4271	3095	0.07 (0.02)	152 (18)	0.05	0.95	0.12 (0.04)	367 (68)	0.17	0.83	0.16 (0.05)	533 (115)	0.17	0.83	0.19 (0.06)	680 (126)	0.12	0.88
10	6286	7201	0.07 (0.03)	158 (24)	0.02	0.98	0.1 (0.05)	422 (86)	0.02	0.98	0.14 (0.07)	748 (180)	0.04	0.96	0.18 (0.08)	1063 (295)	0.09	0.91
11	5969	7271	0.04 (0.01)	137 (19)	0.01	0.99	0.06 (0.01)	381 (61)	0.04	0.96	0.08 (0.02)	695 (134)	0.03	0.97	0.10 (0.02)	1025 (226)	0.03	0.97
12	3154	5150	0.06 (0.03)	110 (45)	0.03	0.97	0.1 (0.04)	274 (117)	0.05	0.95	0.14 (0.04)	404 (179)	0.08	0.92	0.17 (0.05)	486 (207)	0.07	0.93
14	5564	5891	0.07 (0.02)	118 (41)	0.05	0.95	0.10 (0.03)	328 (125)	0.17	0.83	0.13 (0.04)	590 (240)	0.25	0.75	0.16 (0.05)	842 (361)	0.27	0.73
15	2328	1428	0.05 (0.01)	135 (22)	0.03	0.97	0.09 (0.02)	339 (67)	0.12	0.88	0.12 (0.02)	557 (137)	0.21	0.79	0.16 (0.03)	717 (203)	0.3	0.7
16	3440	4507	0.08 (0.06)	158 (37)	0.03	0.97	0.12 (0.1)	403 (120)	0.06	0.94	0.17 (0.13)	670 (235)	0.07	0.93	0.23 (0.16)	917 (374)	0.1	0.9
17	3813	4645	0.05 (0.02)	129 (41)	0.06	0.94	0.07 (0.03)	342 (130)	0.1	0.9	0.1 (0.04)	593 (248)	0.06	0.94	0.13 (0.05)	841 (371)	0.06	0.94
18	1925	983	0.08 (0.04)	90 (58)	0.12	0.88	0.12 (0.05)	233 (157)	0.35	0.65	0.15 (0.06)	379 (262)	0.37	0.63	0.19 (0.07)	499 (346)	0.27	0.73
19	4323	7261	0.06 (0.02)	121 (33)	0.02	0.98	0.08 (0.02)	314 (96)	0.06	0.94	0.12 (0.03)	526 (177)	0.11	0.89	0.15 (0.03)	670 (249)	0.13	0.87

512

513

https://doi.org/10.5194/acp-2020-225
Preprint. Discussion started: 17 March 2020

Atmospheric Chemistry and Physics Discussions

514 **Table 4:** Derived S_{max}, N_d, σ_w for all research flights along with the estimated contribution of each
515 parameter to the variability of the droplet number.

Flight	σ_w (m s^{-1})	$\frac{\Delta\sigma_w}{\sigma_w}$	S_{max} (%)	N_d (cm^{-3})	$\frac{\Delta N_d}{N_d}$	Contrib. κ	Contrib. N_a	Contrib. σ_w
4	1.03±0.25	0.243	0.29±0.19	707±343	0.485	4%	79%	17%
5	0.97±0.1	0.103	0.17±0.10	1040±350	0.337	7%	69%	24%
6	0.94±0.18	0.191	0.13±0.07	1108±283	0.255	3%	54%	43%
9	0.23±0.02	0.043	0.10±0.03	309±51	0.165	7%	76%	17%
10	1.22±0.11	0.090	0.12±0.03	1177±271	0.230	1%	90%	9%
11	1.08±0.04	0.037	0.11±0.03	1082±242	0.224	1%	83%	16%
12	1.05±0.07	0.067	0.18±0.05	495±210	0.424	2%	96%	2%
14	0.85±0.2	0.024	0.15±0.04	761±321	0.422	9%	72%	19%
15	0.28±0.04	0.143	0.08±0.02	321±63	0.196	7%	51%	42%
16	0.20±0.04	0.200	0.10±0.08	289±79	0.273	2%	65%	33%
17	0.71±0.26	0.366	0.15±0.11	742±280	0.377	1%	71%	28%
18	0.90±0.06	0.067	0.31±0.18	538±325	0.604	7%	83%	10%
19	0.99±0.31	0.313	0.15±0.03	699±248	0.355	4%	88%	8%

516

https://doi.org/10.5194/acp-2020-225
Preprint. Discussion started: 17 March 2020

Atmospheric Chemistry and Physics Discussions

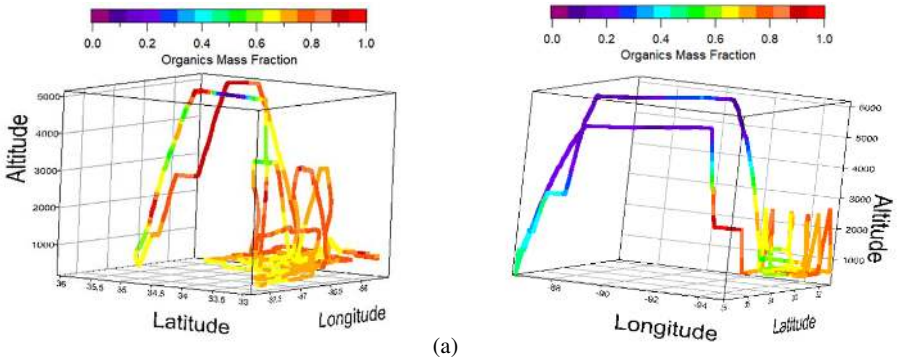

517 **Figure 1:** Spatial and vertical distribution of the organics mass fraction (a) for Flight 5 and (b) for Flight
518 12, denoting the difference in chemical composition, which in turn, may influence cloud droplet number
519 concentration. The color scale denotes the percentage of the organics mass fraction.

520

https://doi.org/10.5194/acp-2020-225
Preprint. Discussion started: 17 March 2020

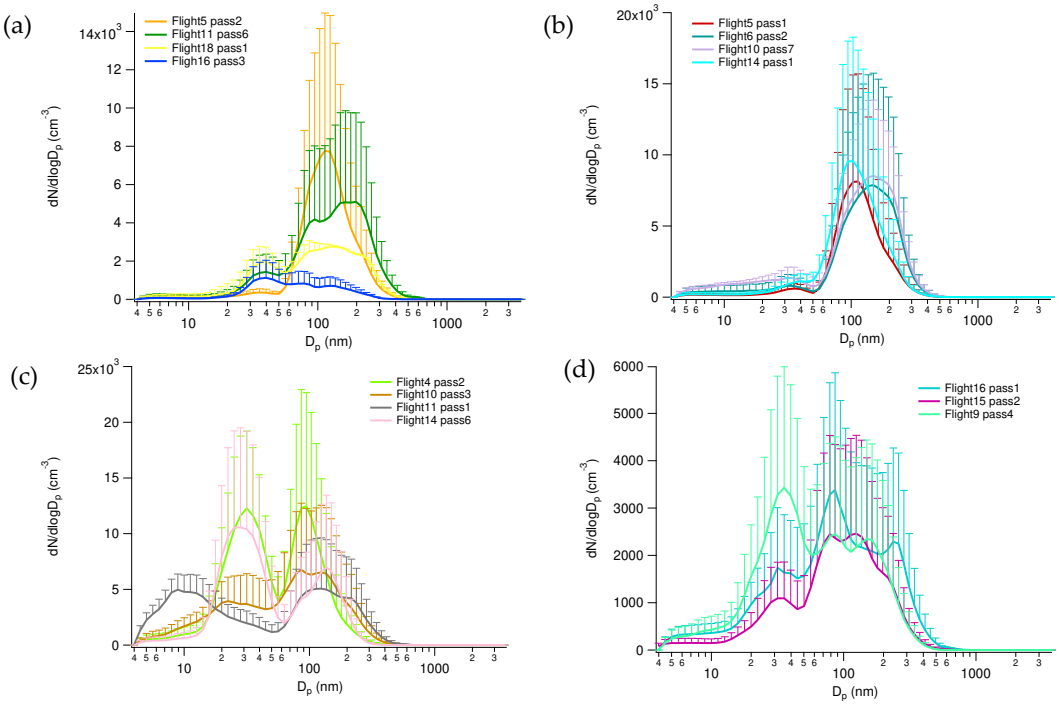

Figure 2: Average particle number size distributions for: (a) free tropospheric conditions, (b) within the boundary layer, (c) for flights with high variability in total aerosol number, and (d) during nighttime flights. Error bars represent the 75th percentile of the distributions within each pass.

https://doi.org/10.5194/acp-2020-225
Preprint. Discussion started: 17 March 2020

Atmospheric Chemistry and Physics Discussions

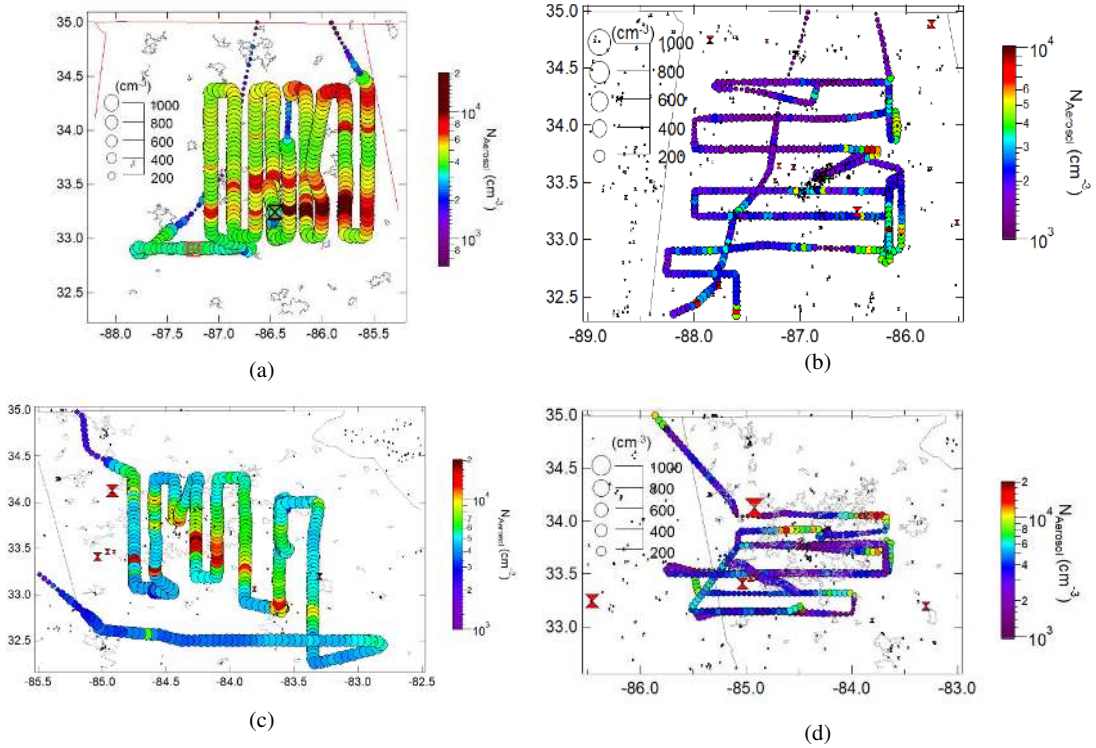

Figure 3: Flight trajectories showing cloud droplet number (indicated by marker size (cm^{-3})) and total aerosol number (indicated by marker color) for the observed characteristic vertical velocity (w^*). (a) for the Alabama sector during daytime (Flight 5) and (b) nighttime (Flight 15). (c) for Atlanta during daytime (Flight 6) and (d) nighttime (Flight 9). Note that the data are plotted at less than 1 Hz in order to better show the size and color of the markers.

https://doi.org/10.5194/acp-2020-225
Preprint. Discussion started: 17 March 2020

Atmospheric Chemistry and Physics Discussions

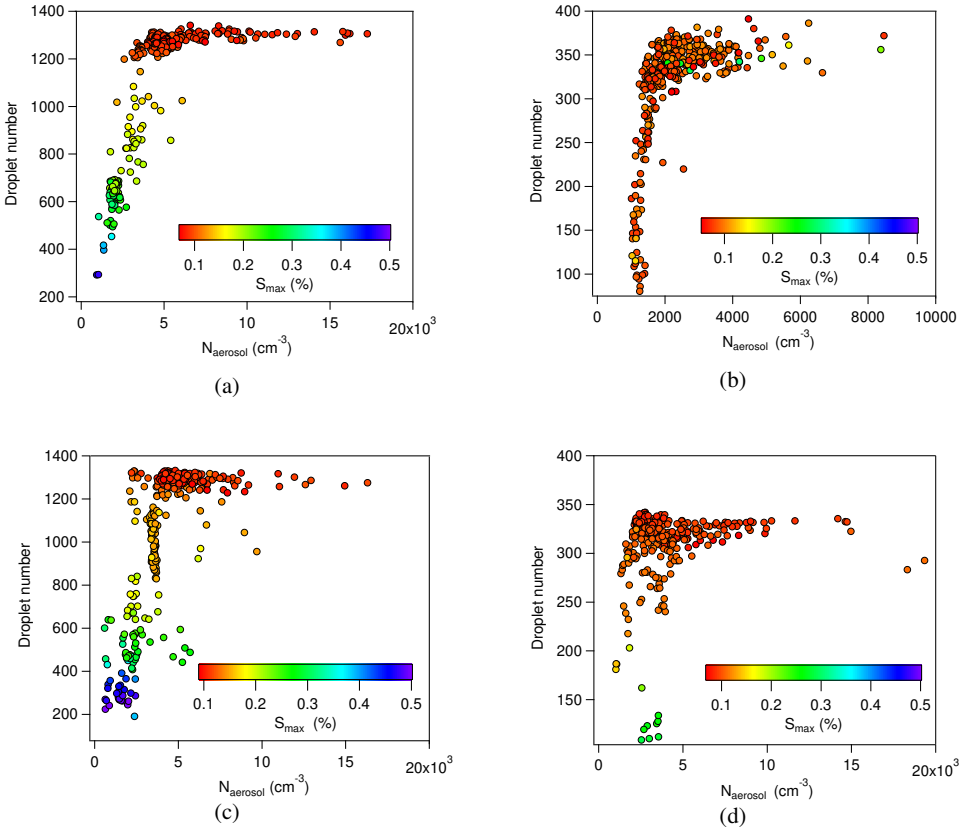

537

538 **Figure 4:** Cloud droplet number vs. total aerosol number for the derived characteristic vertical velocity
539 (w^*). (a) for the Alabama sector during daytime (Flight 5) and (b) nighttime (Flight 15). (c) for Atlanta
540 during daytime (Flight 6) and (d) nighttime (Flight 9). Data are colored by maximum supersaturation.

541

542

543

https://doi.org/10.5194/acp-2020-225
Preprint. Discussion started: 17 March 2020

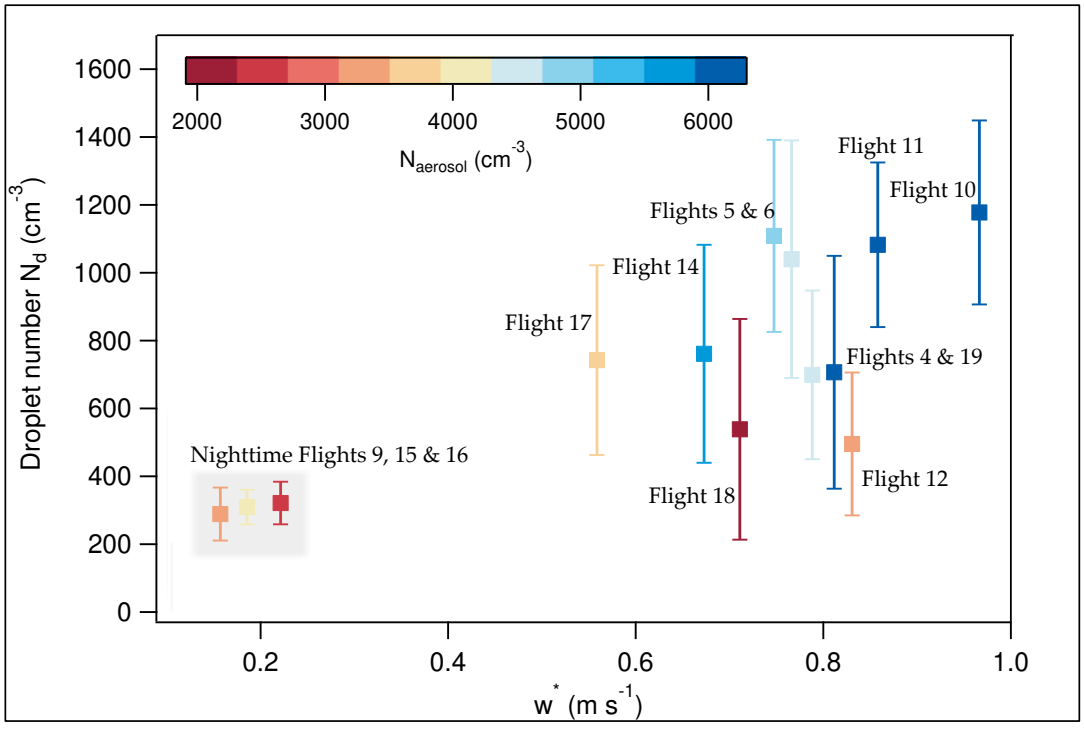

Figure 5: Average cloud droplet number vs. characteristic velocity during the 13 research flights, colored by total aerosol number. Error bars represent the standard deviation of cloud droplet number during each flight. The shaded area represents the flights conducted during nighttime.

https://doi.org/10.5194/acp-2020-225
Preprint. Discussion started: 17 March 2020

Atmospheric Chemistry and Physics Discussions

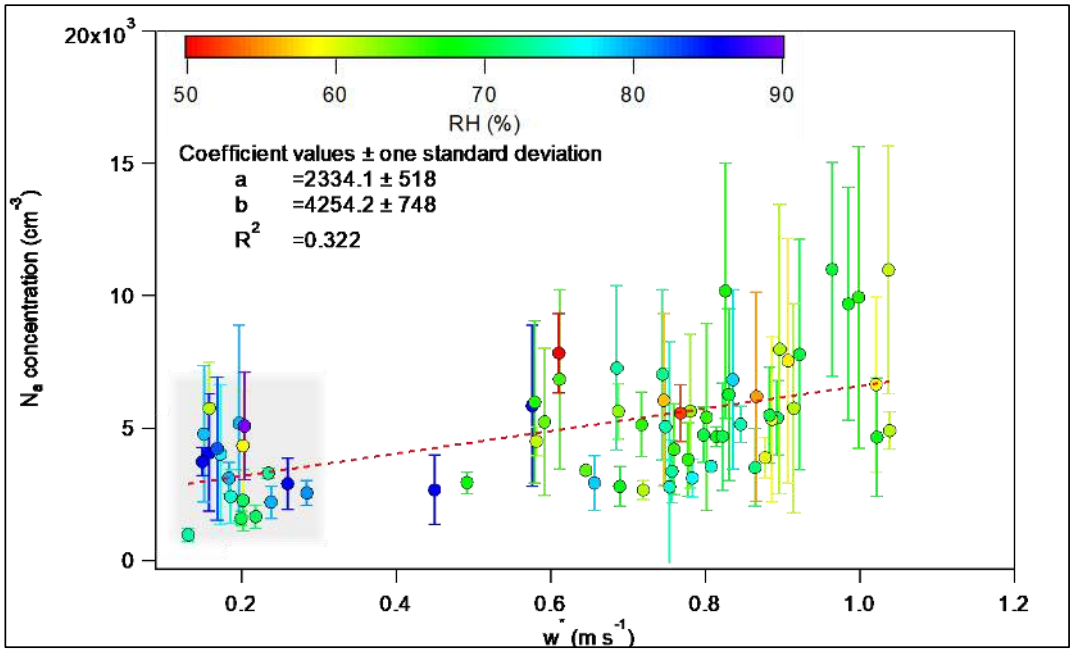

550

551 **Figure 6:** Total aerosol number vs. characteristic velocity during the segments of the flights when the
552 aircraft remained at a constant altitude within the boundary layer, colored by relative humidity. The shaded
553 area represents the segments of the flights conducted during nighttime.

554